Clean Technologies and Environmental Policy (2025) 27:1205–1225
https://doi.org/10.1007/s10098-024-02928-6

ORIGINAL PAPER

Agricultural low-cost waste adsorption of methylene blue and modelling linear isotherm method versus nonlinear prediction

Senem Yetgin[1] · **Merilyn Amlani**[1,2]

Received: 25 March 2024 / Accepted: 7 July 2024 / Published online: 29 July 2024

Abstract

This study shows that geographically marked wheat hull, named *Siyez*, rice hull *Sarı Kılçık*, and *Taşköprü Garlic* stalk were used as agricultural waste to potential adsorbent materials for removing methylene blue from aqueous solution. Experimental data were evaluated in both equilibrium batch process and kinetic studies. In addition, the factors that affect the adsorption capacities, such as pH solutions, methylene blue concentration, contact time, and temperatures, were also investigated. Obtained data were subject to two constant adsorption models of Langmuir, Freundlich, Temkin, and Dubinin−Radushkevich. The kinetic models (pseudo-first-order, pseudo-second-order, intra-particle diffusion and film diffusion) and thermodynamic parameters were evaluated. The adsorption isotherms, characterized by an excellent fit with the Langmuir model ($R^2 = 0.99$) across all adsorbents, underscore the prevalence of monolayer adsorption of methylene blue, in contrast to the Freundlich equation. Adsorption kinetics of the methylene blue onto the adsorbents followed pseudo-second-order kinetic model. According to high regression coefficient (R^2) and minimal values of nonlinear error functions like RMSE; the maximum monolayer adsorption capacities of wheat hull, rice hull and garlic stalk were found to be 62.50 (mg/g), 54.94 (mg/g), and 370.37 (mg/g), respectively. The results indicated that these proposed adsorbents could be low-cost and effective adsorbents for water purification and have adsorption capacity as much as comparable with the literature. In batch equilibrium studies, the adsorption of methylene blue dye onto the wheat hull, rice hull, and garlic stalk exhibited a significant correlation with temperature, contact time, and initial concentration of methylene blue dye and *Adaptive Neuro-Fuzzy Inference System* algorithm for forecasting overall the system parameter well fitted with these findings with the accuracy of outputs (R^2 about 0.99 for each). Consequently, the thermodynamic analysis revealed that the adsorption process takes place in bulk diffusion by liquid phase mass transfer and occurred spontaneously with endothermically except garlic stalk. Adsorption thermodynamic studies show that the adsorption of methylene blue onto the garlic stalk was spontaneous and exothermic.

✉ Senem Yetgin
syetgin@kastamonu.edu.tr

[1] Department of Food Engineering, Kastamonu University, 37200 Kastamonu, Turkey

[2] Mindanao State University Tawi-Tawi College of Technology and Oceanography, Sanga-Sanga, 7500 Bongao, Tawi-Tawi, Philippines

Graphical Abstract

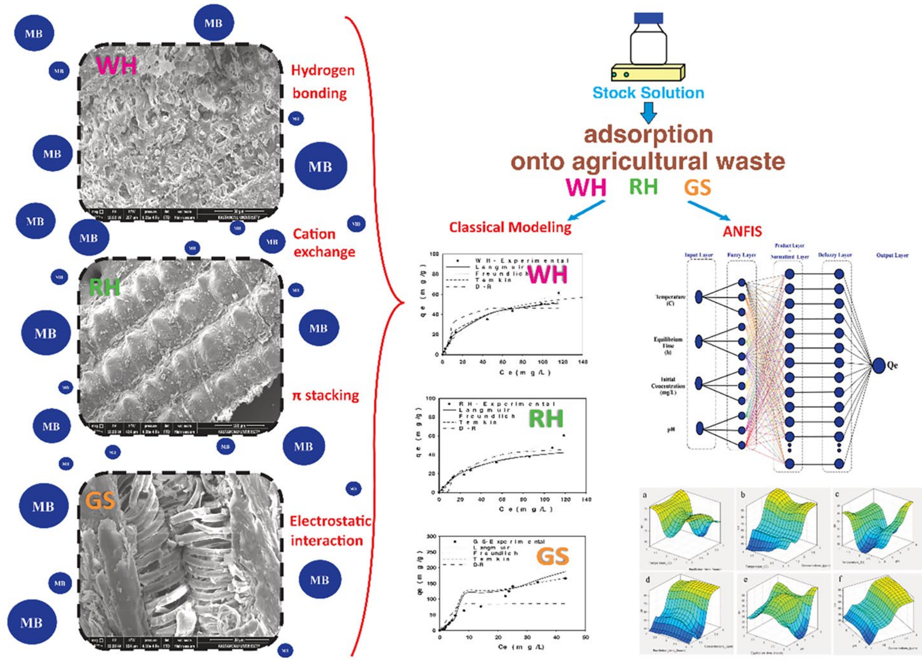

Keywords Methylene blue adsorption · Water purification · Low-cost agricultural wastes · Resource efficiency · Modeling · ANFIS

Abbreviations

ANFIS	Adaptive neuro-fuzzy inference system
ANN	Artificial neural networks
FL	Fuzzy logic
FIS	Fuzzy inference systems
GA	Genetic algorithms
ML	Machine learning
RF	Random forests
SVM	Support vector machines
MF	Membership functions
WH	Siyez–Wheat Husk
RH	Sarı Kılçık–Rice Husk
GS	Garlic stalk
MB	Methylene blue
D–R	Dubinin–Radushkevich
SDGs	Sustainable development goals
MDGs	Millennium development goals
BET	Brunauer–Emmett–Teller
BJH	Barrett–Joyner–Halenda
SEM	Scanning electron microscopy
EDS	Energy-dispersive X-ray spectroscopy
C_0	Initial dye concentrations in the liquid phase (mg/L)
C_e	Dye concentrations in the liquid phase at equilibrium (mg/L)
V (L)	The amount of solution
W(g)	The amount of adsorbent utilized
q_t	The amount of adsorption at time (t) (mg/g)
C_t	The concentration of adsorption at time (t)
S/L	Solid-to-liquid ratio
R^2	Regression correlation coefficient
RMSE	Root-mean-square error
q_e	The amount of adsorbed per unit weight of adsorbent at equilibrium (mg/g)
q_{exp}	The amount experimentally measured
q_{model}	The amount model measured
q_{max}	Maximum adsorption capacity (mg/g)
k_l	Langmuir adsorption equilibrium constant (L/mg)
k_f	Freundlich constant indicating adsorption capacity
n	Freundlich model empirical constant
$\boldsymbol{k_t}$	Temkin isotherm equilibrium binding constant (L/g)
b	Temkin model constant
B	Temkin model constant related to the heat of sorption (J/mol)
T	Temperature (°C, °K)
R	Universal gas constant (8.314 J/mol/K)

q_s	D-R model theoretical isotherm saturation capacity (mg/g)
β	Dubinin–Radushkevich isotherm constant (mol^2/kJ^2)
ε^2	Dubinin–Radushkevich isotherm constant
t	Time (min)
PFO	Pseudo-first order
PSO	Pseudo-second order
k_1	The equilibrium rate constant in the PFO model (g/mg min)
k_2	The equilibrium rate constant in the PSO model (g/mg min)
$\Delta G°$	Gibbs free energy of change
$\Delta H°$	Enthalpy of change
$\Delta S°$	Entropy of change
K_c	Equilibrium constant
MF	Membership function

Introduction

Water is a valuable resource covering 70% of the earth's surface and is vital to human and animal survival. It is also crucial in the manufacturing process and the environment. As a result, water resource management should be prioritized to make clean and safe water available (Qian 2016). However, over the last decade, the rapid rise of industrialization concerning the increase in the human population has resulted in significant environmental contamination. As a result, water is polluted due to various human activities. In addition, due to the global water demand, substantial emphasis has been paid to wastewater recovery, recycling, and reuse (Labaran et al. 2019).

Water pollution is a growing global concern affecting both developed and developing countries. It directly impacts human and animal health, economic growth, and food security. One of the most crucial aspects of living is determining water quality. Not only is it necessary for survival, but it is also essential for the United Nations' new sustainable development goal. The "*Sustainable Development Goal*" is a framework for ecosystems that is not legally binding. The 17 Sustainable Development Goals (SDGs) were added to the 2030 Agenda for Sustainable Development, commonly known as the Millennium Development Goals (MDGs), on January 1, 2016. It contains 17 primary goals and 169 associated targets. Some are closely tied to water, such as #3 good health, #6 clean water, sanitation life, #15 life on land, and #14 life beneath the water. Therefore, observing natural water sources will be critical to both the SDGs and the future of human life (United Nations, 2024).

Water contamination is caused mainly by anthropogenic activities such as human settlements (due to urbanization) and industries. Furthermore, agribusiness has become some countries' primary source of water pollution (The State of Food and Agriculture, 2021). According to the Food and Agriculture Organization of the United Nations Synthesis report in 2021, approximately 2.250 km^3/year of effluent is anticipated to be discharged into the environment, with 330km^3/year being urban wastewater, 660km^3/year being industrial wastewater that includes cooling water, and the remaining 1.260 km^3/year being agricultural wastewater.

Discharging colored effluents/wastewater from various textile, food processing, cosmetic, and other dyeing industries is a severe environmental management issue, particularly in developing nations. Synthetic dyes such as azo dyes (80%) are extensively used in the industries as mentioned above, particularly in the textile industry (~75% of the global dyestuff consumed), which is one of the largest polluters in the world, approximately 92 million tons of waste discharges per year and around 79 trillion liters of water consumes (Slama et al. 2021). It is also the largest source of highly colored effluents that are being discharged into the bodies of water and may pose a risk to the health of humans and other aquatic life (Chen et al. 2012).

Dye is among the most troublesome pollutants (El-Maghraby & El Deeb 2011). There are around 100,000 commercially accessible dyes, with approximately 8×10^5 tons/ of synthetic dyes produced each year globally, and according to the United States "Color Index," 60,000 tons of dyes were discharged yearly (Said et al., 2020). Because most dyes are resistant to photodegradation, biodegradation, and oxidizing agents, they are difficult to decompose. As a result, treating contaminated colored water is a complex process (Slama et al. 2021).

For the removal of dyes from waste water, several techniques of treatment have been used (Liu, 2020), including oxidation (Ramesh et al. 2021), ozonation (Yuzer & Selcuk 2021), electrolysis (Aydin et al. 2022), reverse osmosis (Zahraa et al. 2021), filtration (Marszałek & Żyłła, 2021), coagulation/flocculation (Goudjil et al. 2021), adsorption (Bokil et al. 2020), membrane process (Silva et al. 2021), ion exchange (Cseri et al. 2021), biodegradation (Srinivasan & Sadasivam 2021), and certain combinations of these processes (Güneş & Gönder 2021). However, because some methods are relatively expensive, and some may clog, limiting color removal, adsorption is often employed and favored (Adane et al. 2021). The adsorption method is preferred over other wastewater dye treatment methods because of its advantages: high efficiency, low cost, simple operation, and insensitivity to harmful compounds (Kuang et al. 2020). The adsorbent's amount of adsorbate taken up per unit mass (or volume) of the adsorbent is known as adsorption capacity. Activated carbon is a prominent adsorbent used for water and industrial wastewater treatment. It has good features like high surface area, high porosity, and high adsorption due to its microporous structure (Philippou et al., 2023). Other adsorbents utilized in adsorption include silica gel (Wahshi et al. 2019), activated alumina (Wasti & Ali Awan 2016), polymers and resins (Panic et al., 2013), clay (Adeyemo et al. 2017), and zeolites (Hammood et al. 2021). However, they are all pricey as a result, many researchers are now focusing on developing novel low-cost adsorbents, such as agricultural waste biomass, that can be utilized as an alternate method of treating contaminated waters (Rafatullah et al. 2010). Agricultural waste biomasses, such as garlic peel (Hameed & Ahmad 2009), wheat husk (Banerjee et al., 2014), rice husk (Sawasdee et al., 2017), pomelo peel (Zhang et al., 2018), mandarin peel (Park et al. 2021), guava leaf powder (Aly et al., 2019), banana leaf (Solangi et al., 2021), palm ash and oil palm ash soya (Mittal et al., 2005) and many other alternative sorbents (Rafatullah et al. 2010), are being used in adsorption methods because of their lignocellulosic biomass characteristics (Bhatnagar et al., 2015) and due to their abundance and low cost (Gupta 2009).

This study used lignocellulosic agricultural waste biomass such as rice hull, wheat hull, and garlic stalk as possible adsorbents for treating wastewater using adsorption methods. These three agricultural products are geographically marked and have recently become very popular in production and marketing. Additionally, these agricultural waste biomasses are readily available due to their high consumption, which has resulted in massive amounts of waste being disposed of, which can cause severe problems for the community, especially when not managed properly or burned in the open air, which causes another type of pollution (Shaikhiev 2022).

On the other hand, to be able to compare the superiority of new adsorbents against each other in dye adsorption, it is necessary to limit the type of adsorbed dye as much as possible. For this reason, there are a wide variety of studies on methylene blue (MB) for cellulosic materials and newly synthesized adsorbents and comparison of their MB adsorption capacities provides great convenience to researchers low cost labeled (Fadzail et al., 2022), silica composites PVC (Yetgin et al. 2015), some agricultural waste like rice husk, (Chen et al. 2012), pomegranate peel (Ahmad et al. 2021), orange peel (Gunay Gurer et al. 2021), leaves (Makeswari et al. 2016), and edible fungi (Bo et al. 2021), ash briquette (Sareen et al., 2014) which are some of them. Furthermore, MB serves as a cationic dye and is extensively employed in calico printing, cotton dyeing, leather tanning, and leather dyeing (Makeswari et al. 2016). MB was subjected to many studies about its potential side effects, such as methemoglobinemia, tissue necrosis, mental confusion, and vomiting of MB toxicity (Kumari et al. 2023), and also two adverse environmental impacts of dyes include restricting oxygen transfer and impeding sunlight penetration into water bodies (Patil et al. 2020). Therefore, the removal of MB from aqueous media is inevitable and essential from a sustainable development point of view.

At this point, it is helpful to remember that many parameters affect the success of the adsorption process. The surface area of the adsorbent, surface charge, isoelectric point of the solution, pH, temperature, equilibrium time, concentration difference, which is the driving force of mass transfer and many more affect the adsorption process's success. Due to the limitations of their model assumptions, more than classical linearization models are needed to give all these parameters in a single direction. For this reason, machine learning (ML) methodologies have recently been used to give more realistic results by testing all experimental parameters within themselves for adsorption. Recently, soft computing methods such as artificial neural networks (ANN), fuzzy logic (FL)-based techniques (i.e., fuzzy inference systems, FIS), genetic algorithms (GA), and several connectionist systems such as adapted neuro-fuzzy inference systems (ANFIS) are increasingly being recognized as accurate learning schemes for modeling complex phenomena in different aspects of engineering, physical, and natural sciences. Comparing the proximity of experimental data to the predictions generated by the ML models can swiftly assess the performance of machine learning algorithms. Some examples of supervised learning algorithms include artificial neural networks (ANN), random forests (RF), support vector machines (SVM), and lazy learner algorithms (Duranoğlu et al. 2024).

Within the realm of artificial intelligence (AI) lies ANFIS, which combines the learning abilities of ANN with the reasoning capabilities of fuzzy systems. It comprises five layers, each serving distinct functions: a fuzzy layer, a product layer, a normalized layer, a defuzzy layer, and a total output layer (Abedini et al. 2011). This integration affords ANFIS the advantages of both models within a single methodology (Dolatabadi et al. 2018). Compared to employing a single methodology through a combination of fuzzy systems and artificial neural networks, ANFIS presents a more efficient approach in numerous engineering applications. ANFIS finds application in adsorption modeling by leveraging experimental data from the adsorption process. The output variable is typically the quantity of adsorbate adsorbed. Subsequently, ANFIS can predict the adsorption capacity of the adsorbent across various operational scenarios. ANFIS processes data inputs using membership functions (MF) to estimate outcomes, blending the adaptability of fuzzy logic with the learning capacity of neural networks. Therefore, the literature includes many studies related to the ANFIS fuzzy logic system including dye and other substance adsorption such as Basic Red46 (BR46) and Cu adsorption onto sawdust (Dolatabadi et al. 2018), Cr(VI), Cd, Pb adsorption onto soil ceria (Agbaogun et al. 2023), modified cellulose nanocrystals–sodium alginate or other nanoparticles (Banza et al. 2023), hexavalent chromium adsorption by activated eucalyptus biochar (Yusuff et al., 2023), urea herbicide by soil, heavy metal onto active carbon (Nwosu-Obieogu et al. 2022), methyl orange onto magnetic chitosan (Tanhaei et al. 2017), violet dye onto agricultural waste (Nayak & Pal 2021), MB onto *Azolla pinnata* (Kooh et al. 2022), malachite green onto *Artocarpus odoratissimus* leaves (Zaidi et al. 2018).

In this study, lignocellulosic agricultural waste biomasses were investigated as potential adsorbents without any pretreatment to avoid extra energy and chemical consumption for removing the dye of methylene blue (MB) from aqueous solutions. However, traditional adsorption processes may not fully capture the complex interactions between adsorbate and adsorbent, necessitating advanced modeling techniques such as the ANFIS to enhance the understanding and optimization of the adsorption process. ANFIS combines the advantages of neural networks and fuzzy logic to model complex systems, making it suitable for analyzing and predicting the behavior of adsorption processes in wastewater treatment (Fiyadh et al. 2023). By incorporating ANFIS, this study aims to improve the efficiency and effectiveness of dye removal using agricultural waste biomass as adsorbents.

This study introduces a fresh approach to adsorption, employing agricultural waste biomass as affordable adsorbents for dye removal. It stands out for integrating ANFIS modeling to optimize the process, offering a promising solution to environmental challenges and aligning with sustainable development objectives. These distinctive features set it apart from prior research, emphasizing its potential to propel advancements in wastewater treatment technologies. Moreover, it is readily accessible at no cost or a negligible expense, rendering easily obtainable and cost-effective adsorbent.

Table 1 Properties and characteristics of MB (NCBI, 2021)

Generic name	Methylene blue hydrate
Properties and characteristics of methylene blue	
Chemical name (IUPAC)	[7-(dimethylamino) phenothiazin-3-ylidene]-dimethylazanium;chloride;hydrate
Chemical formula	$C_{16}H_{20}ClN_3OS_{aq}$
λ_{max}(nm)	664

Materials and methods

Preparation of adsorbate

Methylene blue (MB) from Sigma-Aldrich (D-89555 Steinheim, 07323/970, Product of India) with a purity <= 100 % was used as an adsorbate. The dye's properties are listed in Table 1 (Gürses et al., 2016). All the solutions were prepared with deionized water obtained from the Milli-Q Ultrapure Water Purification system. Five-point calibrations were performed for the determination of concentrations of MB. The calibration curves' correlation coefficients (R^2) were 0.989 and 0.987 for MB.

Preparation and characterization of adsorbents

In this study, wheat hull (WH) "Siyez"-*einkorn* (*Triticum monococcum*), rice hull (RH) "Sarı Kılçık" *Oryza sativa L*, and *Taşköprü Garlic* stalk (GS) *Allium sativum L* were used as promising low-cost adsorbents. They were obtained from Kastamonu Province, Turkey, as waste from the local farmer without any cost.

Upon arrival, the samples were cleaned and boiled in pure water for 30 minutes before being filtered and dried in a 60 °C oven for 24 hours. The dry materials were next crushed with a blender (Arzum, Prokit 444, Electronic) and sieved to a mesh size between 250–500 µm. Finally, the processed samples were put in an airtight container for future analysis. No other chemical or physical treatments were used before the adsorption trials.

Surface area measurement

Brunauer–Emmett–Teller (BET) for surface area analysis and Barrett–Joyner–Halenda (BJH) (Quantachrome Model: Nova Touch LX4) for pore size and volume analysis of the adsorbents were performed, and findings are shown in Table 2. According to the IUPAC sample porosity (diameter: micropores < 2 nm, mesopores 2–50 nm, macropores > 50 nm) (Chaisuwan, 2011), the adsorbents are mesopore materials, which means that the samples are initially potential adsorbents because porous materials can act as suitable adsorbents for various fluids due to their conductive properties (Heller-Kallai, 2013).

Table 2 Characterization of adsorbents by Brunauer–Emmett–Teller (BET) and Barrett–Joyner–Halenda (BJH)

	Rice hull	Wheat hull	Garlic stalk
Characterization of adsorbents			
Surface area (m^2/g)	0.3943	1.6561	0.0831
Pore volume (cc/g)	0.00578487	0.0099742	0.00328468
Pore diameter (nm)	3.2384	3.25098	3.23044

FTIR analysis

The purpose of employing FTIR analysis is to ascertain the presence of functional groups for selected agricultural waste of the adsorbent species, with the identification of characteristic peaks being derived from prior studies via FTIR spectrophotometer (BRUKER Model: ALPHA). Spectra were obtained with a scan range between 400 and 4000 cm^{-1}.

Observations derived from Figure 1 reveal distinct spectral features that can be estimated as the existence of the following bonds and groups such as 3400–3650 cm^{-1} (O–H), 3020–3100 cm^{-1} (=C–H), 1640–1680 cm^{-1} (C=C) which can have an alcohol O–H group and an alkene double bond. Moreover, the existence of the peaks around 3300 cm^{-1} (≡C–H), 2100–2260 cm^{-1} (C≡C), and 1735 cm^{-1} (C=O) indicated a terminal alkyne triple bond and a saturated ester carbonyl group. Conversely, the minor band observed at 1735 cm^{-1} corresponds to the stretching vibration of carboxyl groups which also indicates a characteristic lignin-associated band (Urruzola et al. 2013). Furthermore, alkane C–H bonds show a strong absorption from 2850 to 2960 cm^{-1}, and saturated C–C bonds show a few bands in the 800 to 1300 cm^{-1} range and =C–H out-of-plane bending absorptions in the 700–1000 cm^{-1} range. Notably, the peak observed at 1265 cm^{-1} signifies the OH in-plane bending of cellulose. Additionally, a minor, sharp band detected at 897 cm^{-1} is representative of glycosidic C1–H deformation, involving contributions from ring vibration and OH bending. This feature is characteristic of glycosidic linkages between glucose and cellulose. Finding figured out that for all cellulosic characteristic bonds, GS has the highest intensity among all selected promising adsorbents in this study.

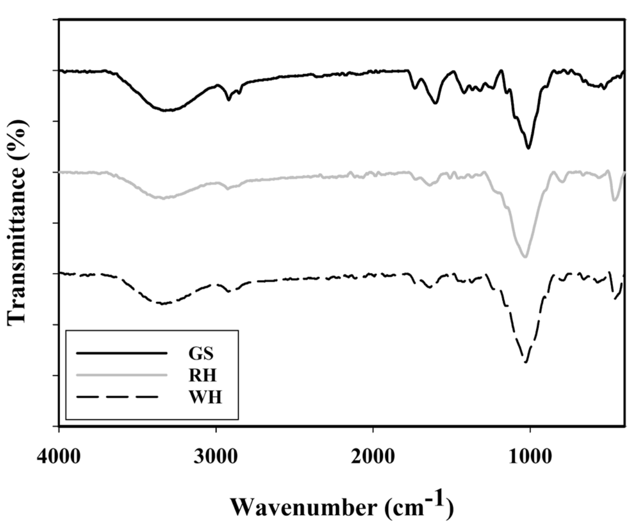

Fig. 1 FTIR spectra of WH, RS, and GS, respectively

Morphology analysis

The structure of the adsorbent materials was investigated to understand the surface and possible inner structure via Quanta (FEG-250) model scanning electron microscopy and energy-dispersive X-ray spectroscopy (SEM/EDS). Figure 2 shows the fracture surface of pretreated adsorbent sieved WH-RH and GS from left to right for every magnification. Each agricultural absorbent has a distinguished structure of fibers. These micro-fibrils are known to be formed by cellulose molecules, chemically associated with glycoproteins, hemicellulose, and acid pectins (Romero-Ocaña et al. 2022). Adsorbents have homogenous fractured surfaces without pores, and some cracks were observed. The surfaces of fibers are generally smooth, presenting, in some cases, some roughness due to the fibrillation. RH shows the cellular tissue whose surface is observed to be the presence of stomas. In GS, high hemicellulose content is seen clearly at increased magnification.

Batch adsorption equilibrium and adsorption kinetic experiments

Batch adsorption equilibrium

A 3g/L solid-to-liquid ratio (S/L) in 10 ml carried out adsorption studies. Therefore, adding a predetermined amount of adsorbents (0.03g) to a series of 50ml flasks filled with 10ml diluted solutions (20–300 mg/L). The flasks were sealed and placed in a water-bath shaker machine (Nükleon, NSCB Series) at 25 °C and 100 rpm for different equilibrium intervals based on WH, RH and GS. After that, the flasks were removed from the water bath. A Spectrophotometer was used to determine the final dye concentration in the solution, with absorbance measured at MB's maximum wavelengths (664nm). The procedure was repeated at least three times. Five-point calibrations were performed for the determination of concentrations of MB. The amount of dye adsorption at equilibrium q_e (mg/g) was calculated using the following formula (see Table 3)

$$q_e = \frac{(C_0 - C_e)V}{W} \quad (1)$$

The kinetic test method was almost equivalent to the equilibrium test method. The aqueous samples were collected at 30-minute intervals, and the dye concentrations were determined similarly. The amount of adsorption at time (t) was determined using the formula of q_t (mg/g) which is the same as q_e at the function of the time.

Nonlinear regression analysis was applied to figure out batch and kinetic model parameters. Evaluations were

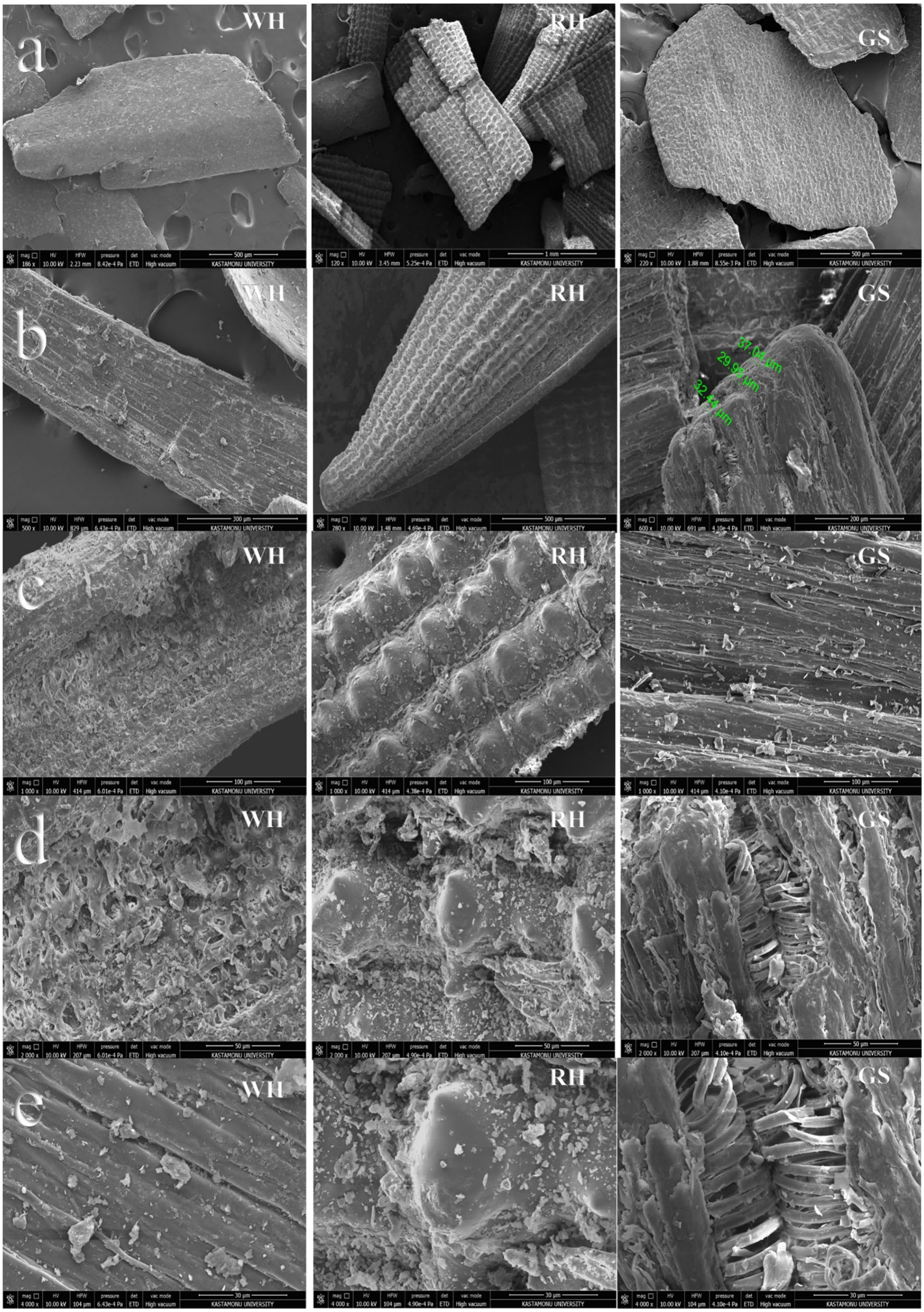

Fig. 2 SEM micrographs of adsorbents WH-RH and GS from left to right at different magnifications **a** about 200x, **b** 500x, **c** 1000x, **d** 2000x, **e** 4000x

Table 3 The formula for equilibrium and kinetic studies

Symbol	Equivalent
C_0(mg/L)	Initial dye concentrations in the liquid phase
C_e(mg/L)	Dye concentrations in the liquid phase at equilibrium,
V(L)	The amount of solution
W(g)	The amount of adsorbent utilized

performed based on two indicators to compare various models representing the same dependent variable (i.e., q for the kinetic models and q_e for the isotherm models): correlation coefficient (R^2) frequently used to choose whether the model is represented correctly versus obtained experimental data and root-mean-square error (RMSE). RMSE is defined as:

$$\mathrm{RMSE} = \sqrt{\frac{\sum_1^N \left(q_{\exp} - q_{\bmod el}\right)^2}{N}} \quad (2)$$

where $q_{\exp}$ and q_{model} are the experimentally measured and model prediction for the amount of MB adsorbed, respectively. A model with a smaller RMSE represents the data more accurately than a model with larger values of this indicator (Table 4).

Adsorption kinetic and thermodynamic

This study used adsorption kinetic studies because they provide essential information about the adsorption mechanism. Adsorption kinetics is referred to as the rate of reaction between adsorbents and adsorbates; it controls the rate of adsorption and the amount of time required to reach equilibrium (Gunay Gurer et al. 2021). The experimental data were examined using pseudo-first-order and pseudo-second-order kinetics (Table 5). Additionally, adsorption thermodynamics were studied based on the listed in Table 6 thermodynamics models.

Effects of initial concentration–contact time–temperature and pH of the solution

To examine the effects of initial concentration and contact time, a 3g/ L solid-to-liquid ratio (S/L) in 10 ml (GS, WH, and RH) was used for MB adsorption. The initial dye solution concentrations tested were 10–300 mg/L, and the studies were carried out at 25 °C for 180 minutes at 30-minute intervals. According to preliminary experimental data, for the GS, the initial concentration of MB was increased to 550 mg/L to reach equilibrium. Additionally, all data were replicated. To investigate the effects of temperature, the studies were carried out for defined equilibrium time intervals at 30 °C, 40 °C, and 50 °C. The data were replicated adsorption procedure which was resumed with the same conditions. All data sets were repeated three times.

The effects of pH solutions were also investigated at pH levels 4, 8, and 12. First, the pH of the solutions was adjusted using HCl (acid) and NaOH (alkaline) and then left overnight to stabilize. Following that, the pH of the solutions was determined, and the adsorption procedure was resumed with the same conditions. All data sets were repeated three times.

Adaptive neuro-fuzzy inference system (ANFIS)

ANFIS is a valuable tool that essentially includes ANN aided with fuzzy logic, used in high-speed modeling of complex nonlinear systems such as control systems, pattern recognition, and forecasting due to the ability to figure out uncertain and imprecise information (Gonzalez del Cerro et al. 2021). Since Jang used it, this system modeling has been extensively used for predicting human knowledge of uncertain systems (Jang 1993). This approach serves a better understanding of the Sugeno model, which also can be used if there is no existing standard method for transforming human knowledge or experience to a fuzzy inference

Table 4 Different types of adsorption isotherms-linear formulas are used for modeling the data

Isotherms	Formula	Assumptions	References
Langmuir	$\frac{1}{q_e} = \frac{1}{C_e k_l q_{\max}} + \frac{1}{q_{\max}}$ Plot: $\frac{1}{q_e}$ Vs $\frac{1}{C_e}$	Monolayer All adsorption sites on the adsorbent are homogeneous Have the same adsorption capacity	Langmuir I. (1917)
Freundlich	$\log_{q_e} = \log_{k_f} + \frac{1}{n}\log_{C_e}$ Plot: $\log_{q_e}$ vs.$\log_{C_e}$	Multilayer adsorption processes Occur on heterogeneous surfaces	Herbert Freundlich (1907)
Temkin	$q_e = B\ln k_t + B\ln C_e$ Where: $B = \frac{RT}{b}$ Plot: q_e vs.ln C_e	As surface coverage increases, the heat of adsorption (ΔH_{ads}) of all molecules in the layer decreases linearly Chemical adsorption process	Johnson and Arnold (1995)
Dubinin–Radushkevich	$\ln q_e = \ln q_s - \beta\varepsilon^2$ Plot: ln q_e vs.ε^2	Express adsorption mechanism on heterogeneous surfaces with Gaussian energy distribution	Dubinin (1989)

Table 5 Different types of adsorption kinetics linear formulas are used for modeling the data

Kinetics	Formula	Assumptions	References
Pseudo-First Order	$\log\left(q_e - q_t\right) = \log q_e - \frac{k_1}{2.303}t$ Plot: $\log\left(q_e - q_t\right)$ vs time q_e and q_t = (mg/g) amount absorbed at equilibrium and at time t = time k_1 = the equilibrium rate constant in the PFO model (L/min)	With time, the dye adsorption rate is proportional to the difference between the amount of dye adsorbed with time and the amount of dye adsorbed at equilibrium	Gunay Gurer et al. (2021)
Pseudo-Second Order	$\frac{t}{q_t} = \frac{1}{k_2 q_e^2} + \frac{t}{q_e}$ $h = k_2 q_e^2$ Plot: $\frac{t}{q_t}$ vs. time h = initial sorption rate q_e = amounts of dye absorbed at equilibrium (mg/g) t = time k_2 = the equilibrium rate constant in the PSO model (g/mg min)	Adsorption is proportional to the square of the difference in the amount of dye adsorbed over time and at equilibrium Chemical sorption, or chemisorption, is the rate-limiting step that predicts adsorption behavior over a wide range of temperatures	Gunay Gurer et al. (2021)
Intra-particle diffusion	$q_t = k_i t^{0.5}$ Plot: q_t vs. $t^{0.5}$ k_i = intra-particle diffusion rate constant	It is believed that the slowest step in the process is the mass transfer from the bulk liquid into the particle's interior, characterized by an intra-particle diffusion coefficient. Meanwhile, external diffusion and surface reaction mechanisms are assumed to occur rapidly	Nayak and Pal (2018)
Liquid-film diffusion	$\ln(1 - F) = -k_{fd}t$ F: fractional attainment of equilibrium, equal to qt /qe	The transport of the solute molecules from the liquid phase up to the solid phase boundary plays the most significant role in adsorption	Sahu et al. (2022)

system and regulating the MF to minimize output error and maximize the prediction performance. This model is also a fuzzy inference system, and ANFIS can be considered an extension or enhancement of the Sugeno method because it incorporates elements of neural networks for learning and adaptation.

The ANFIS architecture consists of at least five layers: the input layer, the membership function layer, the normalized layer, the rule layer, and the output layer. The input layer receives the input variables, and the membership function layer defines the degree of membership of the input variables to each fuzzy set. The normalized layer scales the membership grades to a standard range, and the rule layer combines the rules and computes their firing strengths. Finally, the output layer aggregates the rules' firing strengths to produce the ANFIS system's final output.

ANFIS can be used for adsorption modeling by training it with experimental data on the adsorption process. The output variable would be the amount of adsorbate adsorbed. ANFIS could then be used to predict the adsorption capacity of the adsorbent for different operating conditions. In

Table 6 The equation for the parameters of thermodynamic approaches (Weber 1995)

Parameters	Formula	Assumptions	References
Gibbs free energy of change (ΔG°)	$\Delta G° = -RT\ln K_c$ R = Universal gas constant ($\text{Jmol}^{-1}\text{kg}^{-1}\text{k}^{-1}$) T = Temperature (K) K_c = Equilibrium constant obtained from Khan and Singh Plots: q_e versus $\ln(q_e/C_e)$	Spontaneity Feasibility Negative $\Delta G°$: spontaneous process Positive $\Delta G°$: non-spontaneous Physical adsorption: 0 to − 20 kJ/mol Chemical adsorption: − 80 to − 400 kJ/mol	Weber (1995)
Enthalpy Change (ΔH°) Van't Hoff	$\ln K_c = \frac{\Delta S°}{R} - \frac{\Delta H°}{RT}$ $K_c = \frac{C_a}{C_e}$	Nature and mechanism Positive ΔH: endothermic process Negative ΔH: exothermic process	Weber (1995)
Entropy Change (ΔS°)	R = Universal gas constant $\left(8.314\text{J.mol}^{-1}.\text{K}^{-1}\right)$ T = Temperature (K) K_c = Distribution coefficient C_a = Amount of adsorbate adsorbed at equilibrium $\left(\text{mg.L}^{-1}\right)$ C_e = Equilibrium concentration of adsorbate in solution $\left(\text{mg.L}^{-1}\right)$	Positive ΔS: affinity of the adsorbent toward the adsorbate Increased randomness at the solid/liquid interface (structural changes in the adsorbent and adsorbate)	

this study, adsorption model parameters have been selected as equilibrium time (0–180 mins), temperature (30–40 and 50 °C), initial concentration with different ranges between 10 and 600 mg/L, and pH (5-6-8 and 12) at constant value 3g/L in 10 ml adsorbent, as shown in Figure 3 ANFIS structure for prediction and performed by MATLAB software.

In this study, selecting the input variables is one of the most crucial issues in developing an acceptable forecasting model. Therefore, adsorption model parameters have been selected as equilibrium time, temperature, initial concentration, and pH, as shown in Figure 3 ANFIS structure for prediction.

Results and discussions

The experimental data were analyzed by equilibrium and kinetic models. Four two-parameter isotherm models (Langmuir, Freundlich, Temkin, and Dubinin–Radushkevich (D–R)) and two kinetic models (pseudo-first order and pseudo-second order) were tested. Batch adsorption model isotherms are shown in Figure 4 for WH, RS, and GS, respectively. It depicts the adsorption capacity vs. the concentration at equilibrium at 25 °C. The quantity of dye adsorbed at equilibrium increased from 2.80–61.21 mg/g for WH and 3.24–60.41 mg/g for RS when dye concentration increased from 10–300 mg/L, respectively. For GS, however, concentration equilibrium was reached at 550 mg/L, and the amount of dye removed from 10–550 mg/L concentrations increased from 2.89 to 165.84 mg/g. It demonstrates that increasing the initial dye concentration enhanced the adsorption capacity of the adsorbents. This response was most likely caused by an increase in the driving force of the concentration gradient for mass transfer as the initial dye concentration increased.

The WH, RH, and GS equilibrium data and linear isotherm model predictions for MB are presented in Figure 4. Symbols represent experimental data, whereas lines indicate model predictions. The isotherm parameters, obtained through linear regression analysis, are detailed in Table 7.

Effects of contact time

Figure 5 depicts the impact of contact time on adsorbent adsorption capacity. As illustrated in the first stage, there is some fast adsorption occurring. It was demonstrated that the adsorption capacity increased with increasing contact time and reached equilibrium within 50–100 minutes at 25 °C. The rate of adsorption is then gradually reduced until saturation is reached. The initial quick phase was most likely due to the abundance of active sites. It could have been caused by physical adsorption or ion exchange at the adsorbent surface. As the number of active sites on the adsorbents reduced, sorption became less efficient in

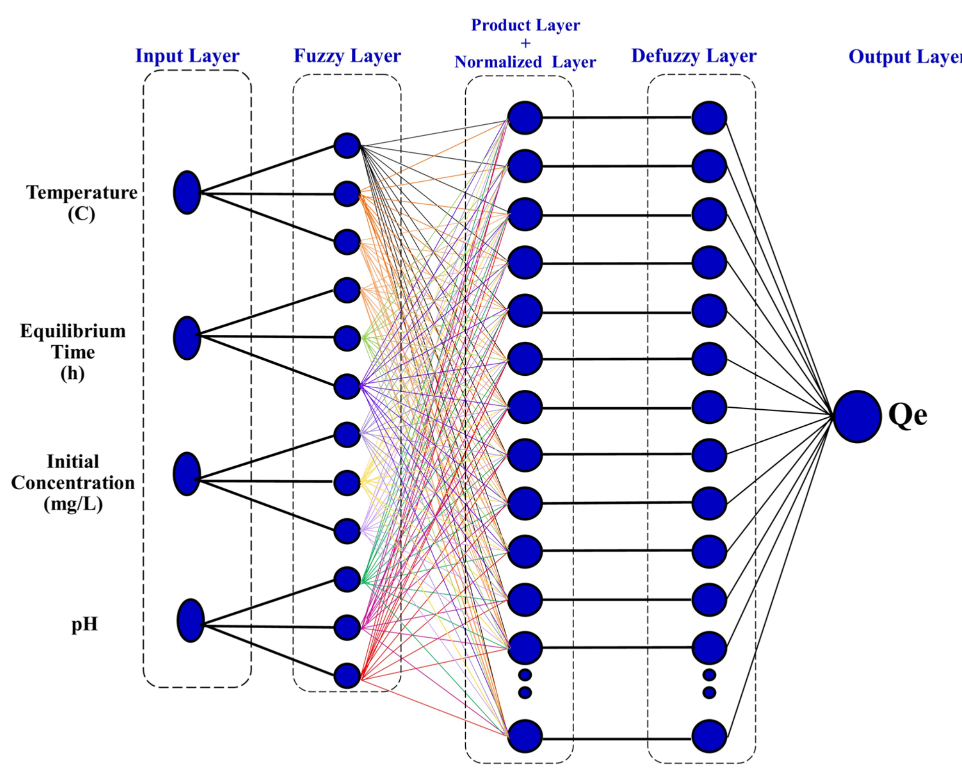

Fig. 3 A five-layer adaptive neuro-fuzzy inference system model for estimating adsorption amount (q_e)

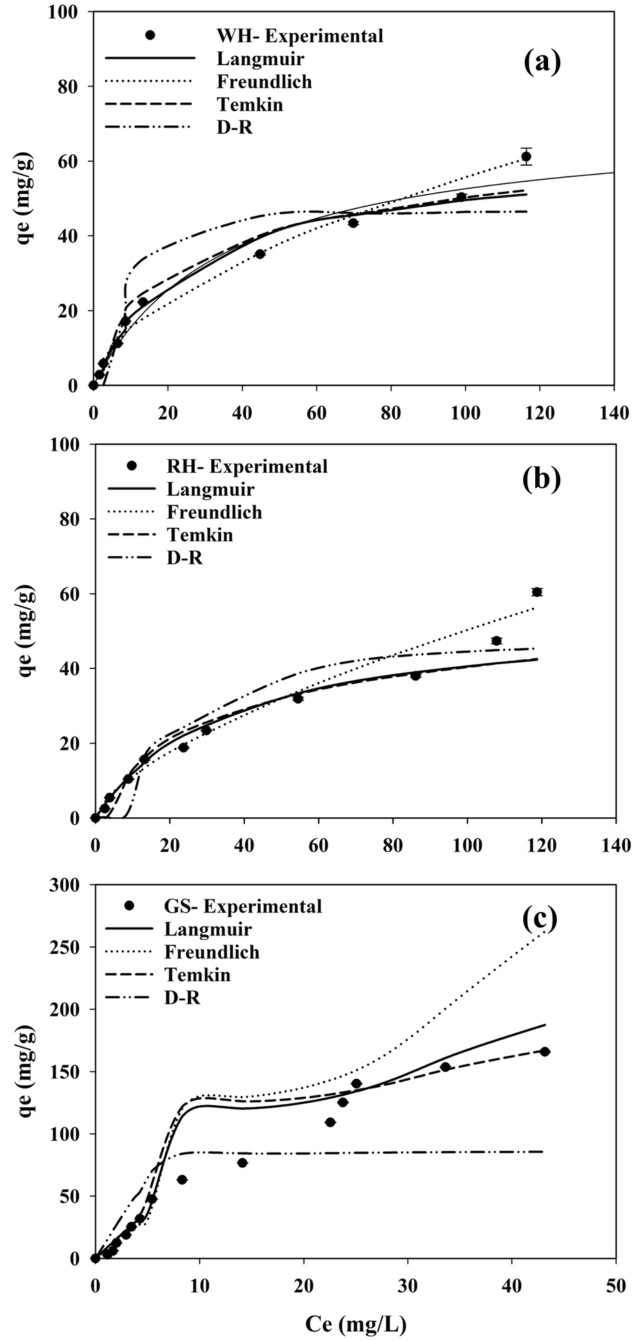

Fig. 4 Experimental equilibrium data and adsorption isotherms: **a** WH, **b** RH, and **c** GS

Table 7 Isotherm parameters of MB adsorption onto different potential adsorbents at 25 °C

Isotherms		WH	RH	GS
Langmuir	q_{max}	62.500	54.945	370.370
	k_L	0.038	0.028	0.020
	R^2	0.993	0.993	0.996
	RMSE	2.082	2.685	4.510
Freundlich	k_f	4.129	2.482	6.479
	n	1.770	1.53	1.07
	R^2	0.968	0.987	0.977
	RMSE	2.291	3.500	7.288
Temkin	k_t	581	0.166	0.415
	b	11.507	12.008	54.249
	R^2	0.975	0.942	0.987
	RMSE	2.963	3.307	7.209
Dubinin–Radushkevich	q_s	46.693	47.371	67.667
	β	223.607	70.711	500.000
	R^2	0.922	0.836	0.963
	RMSE	6.789	5.588	40.425

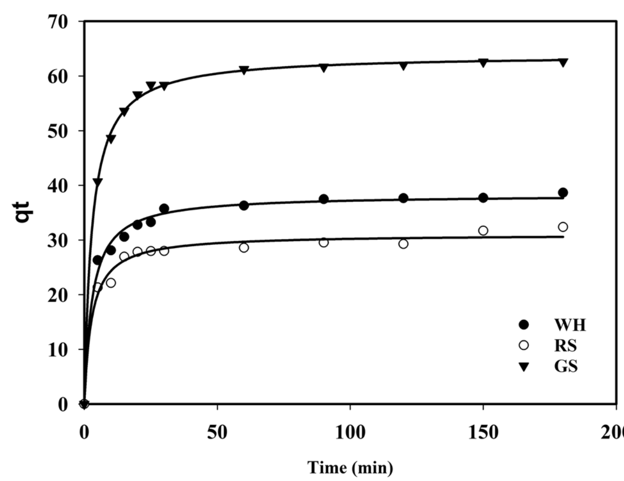

Fig. 5 Effects of contact time for WH, RH, and GS at a concentration of 200 mg/L at a time interval (mins)

the slower stage because additional sorption was impossible once saturation was attained.

Adsorption isotherms (linear)

According to most environmental experts, the demand for low-cost adsorbents to treat contaminated waters is becoming a critical concern. However, predicting the mechanisms of diverse adsorption systems requires modeling experimental data from adsorption processes. As a result, a complete understanding and interpretation of adsorption isotherms are required for the overall enhancement of adsorption mechanism pathways and the practical design of adsorption systems (Ayawei et al. 2017). The adsorbent adsorption of adsorbate and the adsorbate desorption from the adsorbent are the two parts of adsorption. If the rates of the two processes are equivalent (saturation concentration/pressure), adsorption will now enter a dynamic equilibrium condition, and no further adsorption will occur (Kuang et al. 2020). In specific circumstances, such as when the temperature and pH remain constant, the adsorption isotherms are employed to evaluate the relationship between equilibrium adsorption capacity and equilibrium contaminants concentrations. Adsorption isotherms are used to determine the adsorption behavior, identify potential adsorption mechanisms, and calculate adsorption capacity by different models like Langmuir, Freundlich, Temkin, Dubinin–Radushkevich (Table 7), and others. In recent years, because it quantifies the distribution of adsorbates, analyzes the adsorption system, and verifies the consistency of theoretical assumptions in the adsorption isotherm model, linear regression analysis has become one of the most widely used tools for defining the best-fitting adsorption models (Ayawei et al. 2017; Kuang et al. 2020). As a result, based on the model assumption it can be summarized that MB adsorption onto WH, RH, and GS; at each adsorption site, only one adsorbate can be loaded, adsorption occurs on the energetically equivalent sites and the bonding energy of the adsorbent to the adsorbate should be strong enough to prevent displacement of the adsorbed species. Additionally, there is neither attraction nor repulsion between the adsorbed species.

The equations for adsorption isotherms are listed previously in Table 4. According to modeling based on these models for Langmuir, the values of R^2 obtained from the linear graphs of Fig. 7 were 0.993, 0.993, and 0.996 for WH, RH, and GS, respectively. It established that the adsorption process follows the Langmuir and Freundlich isotherm model, as shown in Fig. 7a–f. The values for q_{max} and k_L are shown in Table 7. For Freundlich, the values of R^2 obtained from the graph were 0.968, 0.987, and 0.977 for WH, RH, and GS, respectively. The values of k_f and $1/n$ were also calculated and are presented in Table 7. The slope $(1/n)$ values showed the adsorbent's surface heterogeneity and adsorption intensity. When the value of $1/n$ is in the range of 0.1–1.0, it is often seen as an indicator of a good adsorption process. The values for $1/n$ in this experiment were within the range, indicating that the adsorption process was favorable. Table 7 also includes the calculated values for Temkin and Dubinin–Radushkevich.

The high value of R^2 suggested that the model parameters were in good agreement. According to the Langmuir adsorption isotherm, the theoretical maximum adsorption capacity of MB on WH, RH, and GS were 62.50, 54.95, and 370.37, respectively. All adsorption isotherm analyses were successful, regardless of the isotherm model utilized. However, the Langmuir model was more consistent. These findings suggested that the adsorbent's MB adsorption sites were homogeneous and compatible with the Langmuir model's assumption. As a result, the adsorption mechanism of MB adsorption by WH, RH, and GS was physical and chemical monolayer adsorption.

A summary of the adsorption model and kinetic evaluation model fits can be seen in Table 8. Recent works related to waste and proper biomass MB adsorption have been listed according to adsorption capacity. WH, RH, and GS adsorb amount of MB is comparable with the literature, and GS has the highest capacity among them as performed in this study. Even without any energy-consuming procedure like ashing, in this study, RH showed better adsorption capacity compared to similar studies (Labaran et al. 2019).

The adsorption of MB dye onto GS without any modifications exhibited a maximum monolayer adsorption capacity of 370 mg/g. As shown in Table 8, this value offers a better adsorption capacity than the adsorbent derived from many

Table 8 Comparison of adsorption capacity of MB dye onto WH, RH, and GS with the literature

Material	Adsorption capacity (mg/g)	Isotherm	Kinetics	References
Wheat hull	62.5	Langmuir	2nd order	This Study
Rice hull	54.9	Langmuir	2nd order	This Study
Garlic stalk	370.4	Langmuir	2nd order	This Study
Rice husk	13.50	Freundlich	2nd order	(Labaran et al. 2019)
Rice hull ash (treated)	50.51	Langmuir	2nd order	(Chen et al. 2012)
Edible fungi	208.3	Langmuir	2nd order	(Bo et al. 2021)
Soybean hulls	169.9	Langmuir	2nd order	(Cusioli et al. 2020)
Pea haulm	167	Temkin	2nd order	(Holliday et al. 2022)
Indian almond	88.6	Freundlich	2nd order	(Hevira et al. 2021)
Wall barley	26.2	–	2nd order	(Al-Mahmoud 2020)
Sugarcane bagasse	9.41	Sips	2nd order	(Siqueira et al. 2020)
Citric acid-modified Ricinus communis Leaves	81.29	Langmuir	2nd order	(Makeswari et al. 2016)
Surfactant (HDTMA-Br)-modified pineapple leaf	192.31	Langmuir	–	(Oyelude 2011)
Pomegranate fruit peel activated carbon (PFPAC)	250	Freundlich	1st order	(Ahmad et al. 2021)
Modified Abelmoschus esculentus seeds	354.08, 412.99, 292.00	The Redlich-Peterson	1st order	(Nayak & Pal 2021)

agricultural wastes used for MB adsorption by modification in the literature.

Conversely, although it gave better results than other agricultural wastes, RH gave the lowest adsorption capacity value for this study. Comparative analysis of these findings with data from studies utilizing different adsorbents derived from diverse agricultural wastes for mostly MB dye removal (see Table 8) suggests the efficacy of GS, WH, and RH orderly as an alternative low-cost adsorbent.

Adsorption kinetics (Linear)

Adsorption typically happens in several distinct stages. Initially, the adsorbate migrates from the solution's bulk to the outer surface of the adsorbent. It then diffuses through a boundary layer to reach the solid surface. Then, it selectively adheres to specific active sites on the adsorbent's surface. Finally, there is intra-particle diffusion as the desired molecules move within the adsorbent, furthering the adsorption process.

This study used adsorption kinetic studies because they provide essential information about the adsorption mechanism. Adsorption kinetics is referred to as the rate of reaction between adsorbents and adsorbates; it controls the rate of adsorption and the amount of time required to reach equilibrium (Hamoudi et al. 2018). The experimental data were examined using pseudo-first-order and pseudo-second-order kinetics. The results are listed in Table 9 for all adsorbents used.

The calculated highest correlation coefficient, R^2, for the MB adsorption onto all potential adsorbents used best fits the pseudo-second-order kinetics, which means that the MB uptake rate is proportional to the number of active sites occupied by the adsorbed dye on the WH, RH, and GS surface. The rate-controlling step is chemisorption, which also coincides with Gunay Gurer et al. 2021 study. However, the poor fitting of the pseudo-first-order kinetic model with experimental data shows that the uptake of MB dye by WH, RH, and GS cannot be treated as physical adsorption, and the process of desorption cannot be ignored. Regarding the RMSE comparison, it was determined that the adsorption model data in this study fit the PSO adsorption kinetics linear modeling better than the PFO model equation.

In addition to the most widely used PFO and PSO kinetic modeling (Revellame et al. 2020), intra-particle diffusion and liquid-film diffusion kinetic modeling were also investigated in this study.

The adsorption mechanism was investigated using the liquid-film and intra-particle diffusion models. The liquid-film diffusion model posits that the movement of adsorbate molecules through a liquid film encasing the solid adsorbent represents the slowest phase in the adsorption process, thus controlling the kinetics of the rate processes (Nayak & Pal 2019).

Table 9 Kinetics parameters of MB adsorption onto different potential adsorbents at 25 °C

	Pseudo-first order					Pseudo-second order			
C_0(mg/L)	q_e(mg/g) exp	q_e(mg/g) cal	$k_1\left(\text{min}^{-1}\right)$	R^2	RMSE	q_e.(mg/g) cal	$k^2\times10^3$ g/(mg min)	R^2	RMSE
WH									
20	5.775	1.673	0.022	0.686	28.8	5.855	0.028	0.994	3.5
60	18.034	6.475	0.019	0.895		18.519	0.006	0.996	
100	27.709	7.495	0.020	0.960		28.490	0.005	0.999	
200	38.647	4.492	0.013	0.937		38.462	0.009	1.000	
300	63.956	14.795	0.004	0.920		56.180	0.004	0.999	
RH									
20	5.376	3.094	0.018	0.969	26.8	5.565	0.018	0.998	2.9
60	15.963	5.923	0.014	0.900		16.667	0.003	0.976	
100	21.173	7.426	0.017	0.899		23.419	0.002	0.955	
200	32.363	4.568	0.004	0.766		29.940	0.016	1.000	
300	56.734	6.421	0.004	0.856		51.282	0.006	0.999	
GS									
40	11.687	1.149	0.020	0.943	79	11.792	0.039	1.000	1.5
100	31.199	3.817	0.025	0.997		31.646	0.014	1.000	
200	62.640	6.580	0.021	0.935		63.291	0.007	1.000	
350	109.931	11.397	0.020	0.854		111.111	0.004	1.000	
550	169.318	35.750	0.024	0.978		172.414	0.001	1.000	

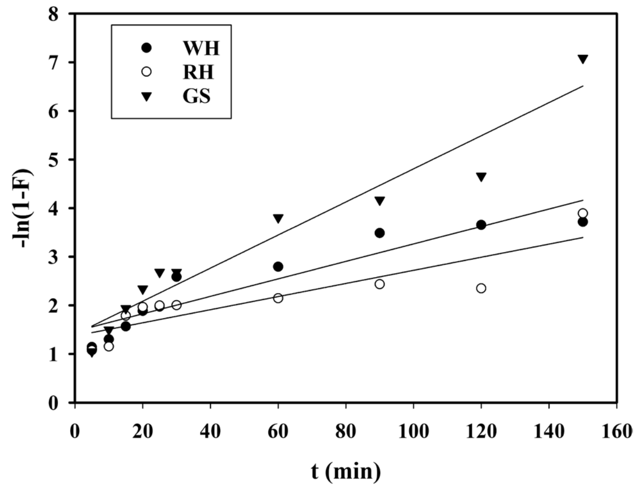

Fig. 6 Liquid-film diffusion kinetic model plots for the adsorption of MB by WS, RH, and GS at 25 °C

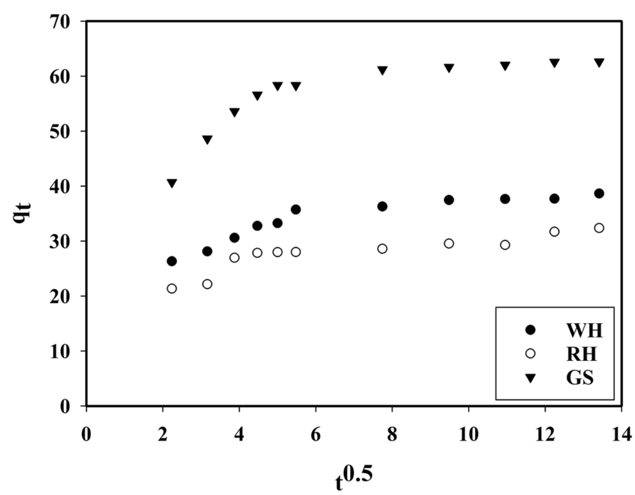

Fig. 7 Intra-particle diffusion kinetic model plots for the adsorption of MB by WH, RH, and GS

A linear plot of ln (1-F) vs. t, exhibiting a zero intercept as shown in Figure 6, suggests that the adsorption process kinetics were governed by diffusion through the liquid film surrounding the adsorbent. However, applying the liquid-film diffusion model to the experimental adsorption data of MB by WH and RH from an aqueous solution at 25 °C revealed unsatisfactory convergence. The resulting plots did not form straight lines passing through the origin and exhibited very low correlation coefficients of 0.84 and 0.79, for WH and RH, respectively. Conversely, for GS, which displayed slightly higher correlation coefficients, the model exhibited better fitting with 0.92. This funding suggests that the diffusion of MB through the liquid film surrounding WH and RH was not the determining factor for the adsorption rate. However, it is worth noting that we applied the liquid-film diffusion model to the initial points, covering the first 25 minutes of adsorption, resulting in slightly improved regression coefficients of 0.94, 0.95, and 0.98. Better correlation might imply that while the liquid-film diffusion model may not govern the adsorption rate entirely, it could still contribute to the process, particularly in the early stage.

In the initial phase, instantaneous adsorption or external surface adsorption occurs. This is followed by the initiation of intra-particle diffusion in the subsequent stage. Finally, the adsorption system progresses toward equilibrium in the final stage. According to the intra-particle diffusion model, the movement of substances from the main liquid body into the inside of the particle happens at a slower pace compared to other steps if it is dominant. This slow movement is defined by something called an intra-particle diffusion coefficient. It is assumed that processes like external diffusion and surface reactions occur quickly. Adsorbate uptake (q_t) varies linearly with the square root of the contact time ($t^{0.5}$) showing whether assumption was obtained or not. Based on this and experimental data evaluation, diffusion steps do not seem to be significant since the line for the intra-particle diffusion equation has not passed from the origin for WH, RH, and GS solid surface adsorption as shown in Fig. 7.

Gibbs free energy change of adsorption

Figure 8 represents the experimental findings of the thermodynamic approach *Kc* have a unit of (1/g), and it was recalculated as dimensionless by multiplying it with 10^3 to have a correct value of ΔG. The Gibbs free energy changes were determined and are listed in Table 10. The negative values of ΔG ranging from 0 to −20 kJ/mol indicate the occurrence of natural adsorption from a thermodynamic perspective, signifying a physically driven adsorption process (refer to Table 6) (Chowdhury et al., 2011). The slope and intercept

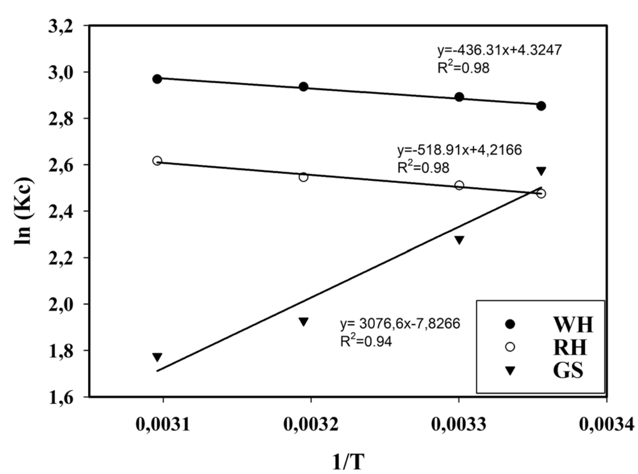

Fig. 8 Van't Hoff plot for the adsorption of MB on WH, RH, and GS at 25, 30, 40, and 50 °C

Table 10 Calculated K and ΔG values for the adsorption of MB on WH, RH, and GS, respectively by using van't Hoff plots equilibrium constant, at 25, 30, 40, and 50 °C

Adsorbent	Temperature (°C)	ΔG (kJ/mol)	ΔH (kJ/mol)	ΔS (kJ/mol)	R^2
WH	25	−17.3	3.62	0.036	0.98
	30	−18.0			
	40	−18.8			
	50	−19.5			
RH	25	−15.0	4.31	0.035	0.98
	30	−12.3			
	40	−12.8			
	50	−13.7			
GS	25	−13.1	−25.58	−0.065	0.94
	30	−9.8			
	40	−6.9			
	50	−5.9			

of the plots depicting ln Kc against 1/T were utilized to ascertain the values of ΔH° and ΔS° (Nayak & Pal 2021). These values were also listed in the same table. The standard free energy change, ΔG °, values for the adsorption of MB dye onto WH, RH, and GS gave negative values at varying temperatures, thus revealing the spontaneity and feasibility of the adsorption process. Additionally, the thermodynamic data show that MB's adsorption mechanism on WH and RS is both physical and endothermic, considering the enthalpy value but not for GS. MB adsorption onto GS is exothermic, and low entropy data represent the reduction of disordering during the adsorption.

Effects of temperature and other thermodynamic studies

The temperature has a significant impact on the adsorption process. As a result, the effect of temperatures was investigated at five different concentrations (20, 80, 150, 250, and 300 mg/L) at four different temperatures (25, 30, 40, and 50 °C). The results are graphed in Figure 9a–c for WH, RH, and GS. The increased temperature resulted in the slightly lower adsorption of higher MB concentration onto the surface of WH, RH, and GS. This indicated that the adsorptions occurred due to a spontaneous endothermic process for WH and RH while exothermic in GS case.

On the other hand, when the adsorption decreases with increasing temperature, it indicates a weak adsorption interaction between adsorbent and adsorbate, supporting physisorption (Bokil et al. 2020). To further understand the process of MB removal by adsorption onto WH, RH, and GS, thermodynamic parameters such as changes in standard free energy ($\Delta G°$), enthalpy ($\Delta H°$), and entropy ($\Delta S°$) were investigated. The values of ($\Delta G°$) for the adsorption of MB on WH, RH, and GS were negative, indicating that the adsorption process is spontaneous at all temperatures. It also indicates that the adsorption is physical because it falls in the 0 to −20 kJ/mol range, indicating physical adsorption. Furthermore, the value of enthalpy change ($\Delta H°$) was also negative for this system, confirming the exothermic nature of the adsorption process. Similarly, low entropy ($\Delta S°$) values confirm the possibility of favorable adsorption.

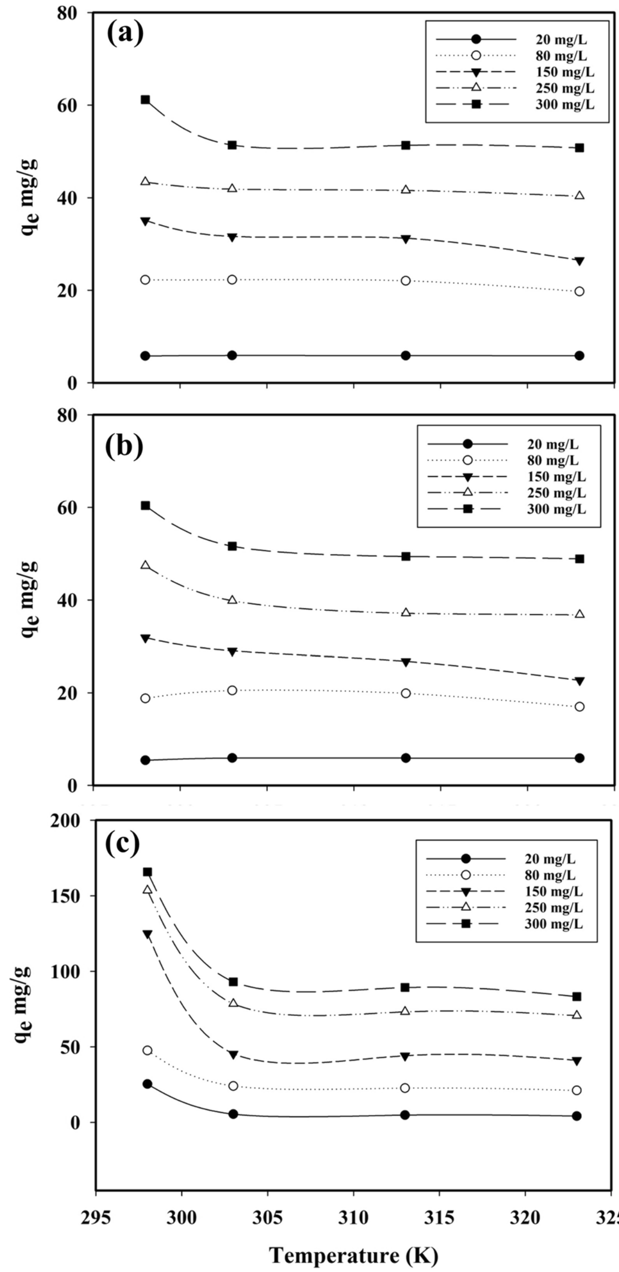

Fig. 9 Effects of different temperatures 25, 30, 40, and 50 (°C) on the adsorption of MB at different concentrations onto **a** WH, **b** RS, and **c** GS

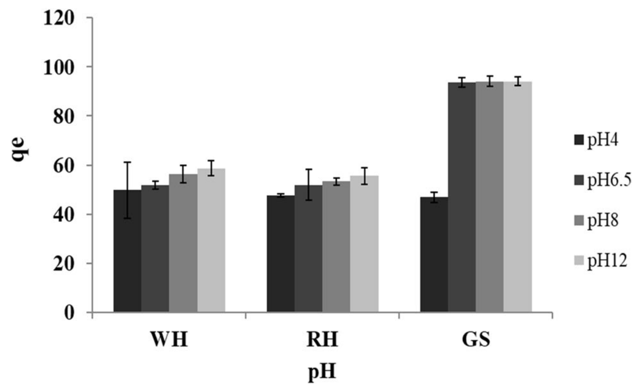

Fig. 10 Effects of pH for wheat hull, rice hull, and garlic stalk at 300 mg/L

Effects of pH solutions

Figure 10 depicts the effect of solution pH on the adsorption capacity of adsorbing MB using WH, RH, and GS adsorbents by the adsorption amounts obtained. The adsorption capacity of the adsorbents was also high at higher pH values due to the availability of more negatively charged surfaces, which caused a decrease in the repulsion between the positively charged MB molecule and the adsorbent (Nayak & Pal 2017). However, at lower pH values, the adsorption capacity of the adsorbents was also low, indicating that in acidic solutions, the high concentration of H^+ ions caused the repulsion and thus reduced the adsorption capacities of the adsorbents. Here, the alkaline degradation of cellulose might influence the adsorption capacity enhancement (Pavasars et al. 2003). It is also indicated that alkaline media produced the *in situ* cellulose nanofibrillation (Merino & Athanassiou 2023). Decreasing the fibril size improves the vacant adsorptive site simultaneously; therefore, the adsorbed amount of MB, as indicated by q_e, increases.

ANFIS results

The primary objective of this study was to optimize the biosorption of MB from aqueous solutions using unmodified agricultural waste as adsorbents, aiming to enhance the removal efficiency of the adsorbate. Examination of the interaction between process parameters and their optimal values can be facilitated effectively through the utilization of three-dimensional response surface plots in Figure 11.

ANFIS 3D surface plots indicate adsorption process parameter correlation with each other with the accuracy of the ANFIS output regression coefficient (R^2) 0.992, 0.993, and 0.996 for WH, RS, and GS, respectively, and all results are consistent with Figure 11a and e. Consequently, the applicability of adsorption data with ANFIS versus selected adsorption input parameters of temperature, equilibrium time, concentration, pH, and output parameter of adsorption capacity were well predicted. Figure 11a signifies even at low-temperature conditions adsorption capacity does not change that much related to as revealed the adsorption mechanism dominated by bulk diffusion of MB onto the surface. Nevertheless, Figure 11b embodies the synergetic interactive effect of temperature increase and solution pH. Besides statistically synergetic interactive influences occur at high temperatures and adsorption is still favorable because of cellulosic structure surface area enlargement by swelling which opens their fibrillar structure during the process (Hribernik et al. 2016). For the same reason, it is shown in Figure 11e that the pH increase provided by using NaOH increases the adsorption capacity.

Mainly as shown in Figure 11b, d and f, concentration is the most dominant input parameter; its rise with any other parameter always results in capacity enhancement in other words under stationary conditions, and the adsorption capacity was low and enhanced at high initial MB concentration. Experiments pH and equilibrium time become ignorable at high initial concentrations with low-temperature values as a manner of adsorb amount. The adsorption capacity enhanced gradually with an increase of initial pH from 7.0 to 9.0 simultaneous temperature increase concerning the active site enhancement onto the surface as discussed in Figure 11c. Still, in high initial concentrations with opposite high temperatures, adsorption is favorable at alkaline conditions with extended equilibrium time (see Figure 11b and c), probably with an alkaline hydrolysis effect on cellulosic construction. Consequently, ANFIS model prediction shows between similar statistical correlation between the adsorption linear model parameters and kinetic analysis model parameters revealed before.

Cost estimation

In this study, all promising adsorbents are waste materials from the agriculture industry. *Sarı Kılçık* (Rice) and *Siyez* (wheat) hulls are abundant as mill waste at no cost, like *Taşköprü Garlic* stalks. On the other hand, activated charcoal, which is currently the most widely used commercial adsorbent for eliminating basic and reactive dyes, is very expensive. The least expensive variant of commercial activated charcoal typically costs approximately 12 USD per kilogram (Sahu et al. 2022). Therefore, employing the suggested adsorbent represents a strategic and cost-effective initiative, tapping into its valuable and essential potential to achieve sustainable development goals and address environmental concerns while lowering the carbon footprint.

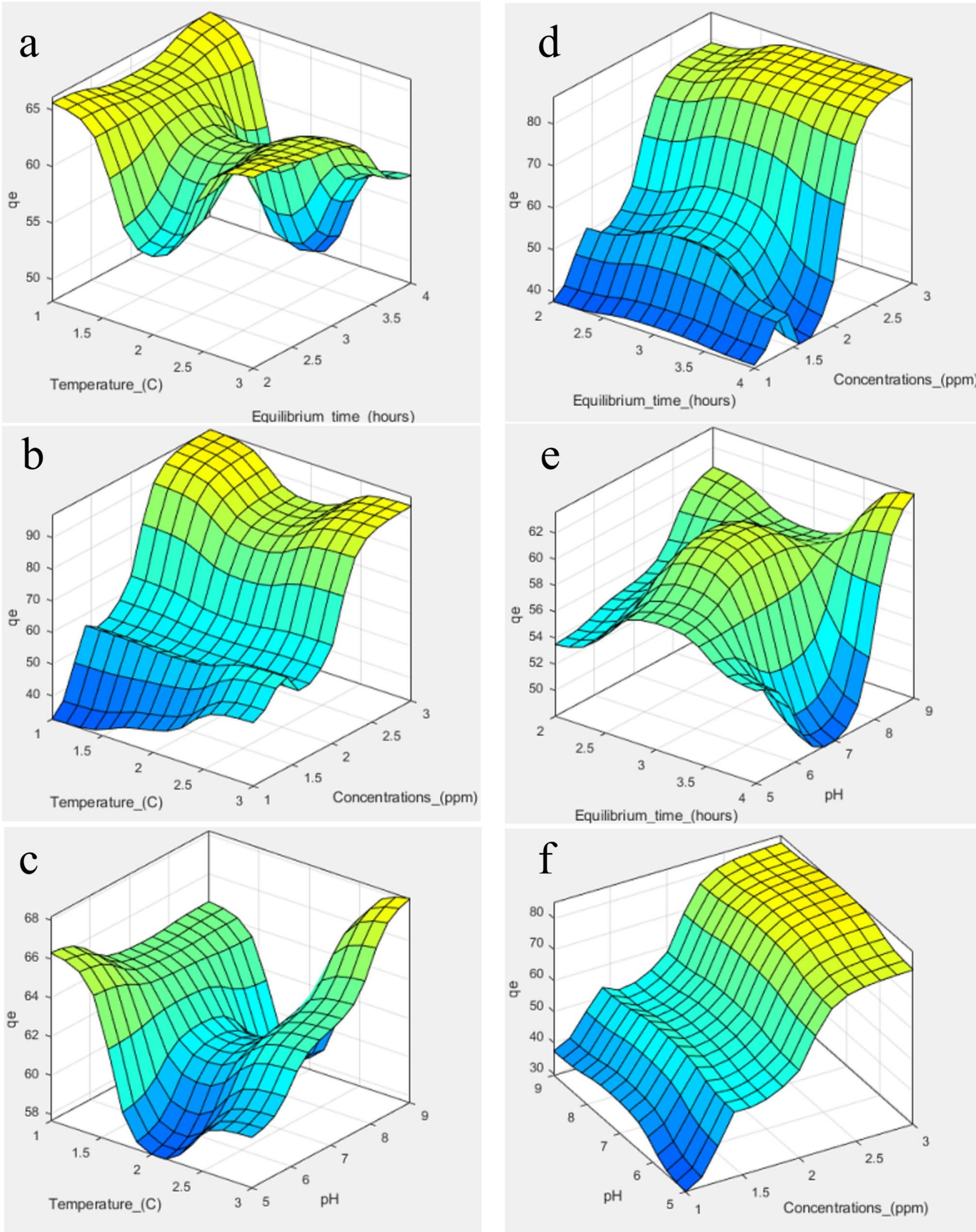

Fig. 11 Surfaces viewer of ANFIS models (**a**) temperature and contact time, (**b**) temperature and MB concentration, (**c**) temperature and solution pH, (**d**) contact time and MB concentration (**e**) contact time and solution pH and (**f**) MB concentration and solution pH

Table 11 Total cost for preparing 1 kg of the adsorbent (32 TL per 1 USD)

Order	Process	Unit cost, USD	Amount used	Net price, USD
1	Boiling	0.046 USD/	2.2 kW/h for 30 min	0.10
2	Drying	0.046 USD	19.2 kW/h (60 °C – 24 h)	0.88
3	Net cost			0.98
4	Other overhead costs (10% of net cost)			0.098
5	Total cost			1.078

Additionally, as shown in Table 11 the total cost for preparing 1 kg of adsorbent is estimated at 1.08 USD. However, the total cost of the adsorbent can be reduced to 0.11 USD by drying the adsorbent naturally at room temperature. Reusability of the adsorbent. Exploring the potential for reusing adsorbents is part of our future research plans.

Conclusions

This systematic investigation furnishes a comprehensive elucidation on the adsorption of MB while also furnishing important insights pertinent to water purification endeavors leveraging potential unmodified agricultural adsorbents like local WH, RH, and GS characterized by their cost-effectiveness and efficacy. These are examples of lignocellulosic agricultural waste biomass that are widely available and discharged in large quantities due to their high consumption of Kastamonu—Turkiye.

These adsorbents were used without any modification and characterized by FTIR, BET, and SEM analysis. FTIR analysis indicates that all adsorbents have a variety of functional groups with GS having the highest intensity- such as hydroxyl, carbonyl, amine, and ester carbonyl groups which might be involved in the adsorption of MB onto the solid surface. The SEM image of GS showed fiber structures trigger the adsorption capacity even has the lowest surface area concerning alkali solution swelling effect. Results also revealed that initial concentration, contact time, solution pH, and temperature have influenced adsorption. It has also been stated that increasing the initial dye concentration and the pH of the solution increased the adsorption capacity supported by mass transfer domination based on chemical potential differentiation and cellulose degradation in alkaline conditions. However, as the temperature rises, the removal rate decreases as the kinetic energy increases. The negative ΔG values confirm that the adsorption is spontaneous and physical. Besides the exothermic behavior of GS reveals the feasibility of adsorption onto the surface not only supports a low-temperature adsorption condition but is also favorable for energy reduction.

Regarding adsorption kinetics, the removal process is governed by pseudo-second-order kinetics (RMSE=1.5) and the Langmuir isotherm ($R^2 = 0.99$) best-fitted data. Therefore, kinetic and equilibrium modeling parameters can be used to design dye wastewater treatment plants. Finally, ANFIS modeling with nonlinear data prediction of adsorption capacity applies to classical adsorption models.

The results indicated that the WH, RH, and GS could serve as low-cost and effective adsorbents for water purification, exhibiting adsorption capacities comparable to those reported in the literature. Moreover, it was observed that their adsorption capacities are significant, with the added advantage of being economically feasible, as their production cost equates to approximately one-tenth that of activated carbon.

Supplementary Information The online version contains supplementary material available at https://doi.org/10.1007/s10098-024-02928-6.

Acknowledgements Kastamonu University, Kastamonu University Central Research Laboratory Funding: Kastamonu University, Scientific Research Projects Coordinatorship, KÜ-BAP01.2018-79. We sincerely thank Dr. Zeynep Gökkuş for her assistance with non-linear regression.

Author contributions Conceptualization and idea: Author A was responsible for developing the initial concept and idea for the study. Methodology: Author A and B designed the methodology used in the study. Validation: Author B conducted the validation of the results obtained from the study. Formal analysis: Author B performed the formal analysis of the data collected. Investigation: Author B conducted the investigation process and gathered data for the study. Data Curation: Author B curated and organized the data for analysis. Writing—original draft preparation: Author B wrote the original draft of the manuscript. Visualization: Author B created visual representations of the data for the study. Writing—review and editing: Author A reviewed and edited the manuscript for clarity and accuracy. Resources: Author A provided the necessary resources for the study to be conducted. Software: Author A developed the software used in the study. Supervision: Author A supervised the overall implementation of the study. Project administration: Author A managed the administrative aspects of the project. Writing—review and editing: Author A reviewed and edited the manuscript to ensure quality and consistency.

Funding Open access funding provided by the Scientific and Technological Research Council of Türkiye (TÜBİTAK).

Data availability The data that support the findings of this study are available from the corresponding author, [Yetgin S], upon reasonable request.

Declarations

Conflict of interest The authors declare that they have no known competing financial interests or personal relationships that could have appeared to influence the work reported in this paper.

References

Abedini R, Esfandyari M, Nezhadmoghadam A, Adib H (2011) Evaluation of crude oil property using intelligence tool: fuzzy model approach. Chem Eng Res Bull 15(1):30–33. https://doi.org/10.3329/cerb.v15i1.7334

Adane T, Adugna AT, Alemayehu E (2021) Textile industry effluent treatment techniques. J Chem 2021(1):5314404. https://doi.org/10.1155/2021/5314404

Adeyemo AA, Adeoye IO, Bello OS (2017) Adsorption of dyes using different types of clay: a review. Appl Water Sci 7(2):543–568. https://doi.org/10.1007/s13201-015-0322-y

Agbaogun BK, Olu-Owolabi BI, Buddenbaum H, Fischer K (2023) Adaptive neuro-fuzzy inference system (ANFIS) and multiple linear regression (MLR) modelling of Cu, Cd, and Pb adsorption onto tropical soils. Environ Sci Pollut Res 30(11):31085–31101. https://doi.org/10.1007/s11356-022-24296-8

Ahmad MA, Eusoff MA, Oladoye PO, Adegoke KA, Bello OS (2021) Optimization and batch studies on adsorption of Methylene blue dye using pomegranate fruit peel based adsorbent. Chem Data Collect 32:100676. https://doi.org/10.1016/j.cdc.2021.100676

Al-Mahmoud SM (2020) Kinetic and thermodynamic studies for the efficient removal of methylene blue using hordeum murinum as a new biosorbent. Egypt J Chem 63(9):3381–3390. https://doi.org/10.21608/ejchem.2020.16008.1970

Ayawei N, Ebelegi AN, Wankasi D (2017) Modelling and interpretation of adsorption isotherms. J Chem 2017(1):3039817. https://doi.org/10.1155/2017/3039817

Aydin MI, Ozaktac D, Yuzer B, Doğu M, Inan H, Okten HE, Coskun S, Selcuk H (2022) Desalination and detoxification of textile wastewater by novel photocatalytic electrolysis membrane reactor for ecosafe hydroponic farming. In Membr 12(1):10. https://doi.org/10.3390/membranes12010010

Banerjee S, Chattopadhyaya MC et al (2014) Adsorption characteristics of modified wheat husk for the removal of a toxic dye, methylene blue, from aqueous solutions. J Hazard Toxic Radioact Waste 18(1):56–63. https://doi.org/10.1061/(asce)hz.2153-5515.0000191

Banza M, Seodigeng T, Rutto H (2023) Comparison study of ANFIS, ANN, and RSM and mechanistic modeling for chromium(VI) removal using modified cellulose nanocrystals-sodium alginate (CNC–Alg). Arab J Sci Eng 48(12):16067–16085. https://doi.org/10.1007/s13369-023-07968-6

Bhatnagar A, Sillanpää M, Witek-Krowiak A (2015) Agricultural waste peels as versatile biomass for water purification - A review. J Chem Eng 270:244–271. https://doi.org/10.1016/j.cej.2015.01.135

Bo L, Gao F, Shuangbao BY, Liu Z, Dai Y (2021) A novel adsorbent auricularia auricular for the removal of methylene blue from aqueous solution: isotherm and kinetics studies. Environ Technol Innov 23:101576. https://doi.org/10.1016/j.eti.2021.101576

Bokil SA, Topare NS, Khedkar SV (2020) Batch adsorption studies on treatment of textile industry effluent using bamboo and green coconut shell activated carbon. IOP Conf Ser: Mater Sci Eng 983(1):012005. https://doi.org/10.1088/1757-899X/983/1/012005

Chaisuwan T (2011) Porous materials from polybenzoxazine. In: Handbook of benzoxazine resins, Elsevier, p 457–468. https://doi.org/10.1016/B978-0-444-53790-4.00071-0

Chen XG, Lv SS, Liu ST, Zhang PP, Zhang AB, Sun J, Ye Y (2012) Adsorption of methylene blue by rice hull ash. Sep Sci Technol 47(1):147–156. https://doi.org/10.1080/01496395.2011.606865

Chowdhury S, Mishra R, Saha P, Kushwaha P (2011) Adsorption thermodynamics, kinetics and isosteric heat of adsorption of malachite green onto chemically modified rice husk. Desalination 265(1–3):159–168. https://doi.org/10.1016/j.desal.2010.07.047

Cseri L, Topuz F, Abdulhamid MA, Alammar A, Budd PM, Szekely G (2021) Electrospun adsorptive nanofibrous membranes from ion exchange polymers to snare textile dyes from wastewater. In Adv Mater Technol 6(10):2000955. https://doi.org/10.1002/admt.202000955

Cusioli LF, Quesada HB, Baptista ATA, Gomes RG, Bergamasco R (2020) Soybean hulls as a low-cost biosorbent for removal of methylene blue contaminant. Environ Prog Sustain Energy 39(2):1–10. https://doi.org/10.1002/ep.13328

Dolatabadi M, Mehrabpour M, Esfandyari M, Alidadi H, Davoudi M (2018) Modeling of simultaneous adsorption of dye and metal ion by sawdust from aqueous solution using of ANN and ANFIS. Chemom Intell Lab Syst 181:72–78. https://doi.org/10.1016/j.chemolab.2018.07.012

Dubinin MM (1989) Fundamentals of the theory of adsorption in micropores of carbon adsorbents: characteristics of their adsorption properties and microporous structures. Carbon 27(3):457

Duranoğlu D, Sinan Altın E, Küçük İ (2024) Optimization of adaptive neuro–fuzzy inference system (ANFIS) parameters via boxbehnken experimental design approach: the prediction of chromium adsorption. Heliyon 10(3):e25813. https://doi.org/10.1016/j.heliyon.2024.e25813

El-Maghraby A, El Deeb HE (2011) Removal of a basic dye from aqueous solution by adsorption using rice hulls. Global Nest J 13(1):90–98. https://doi.org/10.30955/gnj.000560

Fadzail F, Hasan M, Mokhtar Z, Ibrahim N (2022) Removal of naproxen using low-cost *Dillenia indica* peels as an activated carbon. Mater Today: Proc 57:1108–1115. https://doi.org/10.1016/j.matpr.2021.09.422

Fiyadh SS, Alardhi SM, Al Omar M, Aljumaily MM, Al Saadi MA, Fayaed SS, Ahmed SN, Salman AD, Abdalsalm AH, Jabbar NM, El-Shafi A (2023) A comprehensive review on modelling the adsorption process for heavy metal removal from waste water using artificial neural network technique. Heliyon 9(4):E15455. https://doi.org/10.1016/j.heliyon.2023.e15455

Gonzalez del Cerro RT, Subathra MSP, Manoj Kumar N, Verrastro S, Thomas George S (2021) Modelling the daily reference evapotranspiration in semi-arid region of south India: a case study comparing ANFIS and empirical models. Inf Process Agric 8(1):173–184. https://doi.org/10.1016/j.inpa.2020.02.003

Goudjil S, Guergazi S, Masmoudi T, Achour S (2021) Effect of reactional parameters on the elimination of congo red by the combination of coagulation–floculation with aluminum sulfate. Desalin Water Treat 209:429–436. https://doi.org/10.5004/dwt.2021.26474

Gunay Gurer A, Aktas K, Ozkaleli Akcetin M, Erdem Unsar A, Asilturk M (2021) Adsorption isotherms, thermodynamics, and kinetic modeling of methylene blue onto novel carbonaceous adsorbent derived from bitter orange peels. Water Air Soil Pollut 232(4):1–17. https://doi.org/10.1007/s11270-021-05090-7

Güneş E, Gönder ZB (2021) Evaluation of the hybrid system combining electrocoagulation, nanofiltration and reverse osmosis for biologically treated textile effluent: treatment efficiency and membrane fouling. In J Environ Manag 294:113042. https://doi.org/10.1016/j.jenvman.2021.113042

Gupta VK (2009) Application of low-cost adsorbents for dye removal—a review. In J Environ Manag 90(8):2313–2342. https://doi.org/10.1016/j.jenvman.2008.11.017

Gürses A, Açıkyıldız M, Güneş K, Gürses MS (2016) Dyes and pigments: their structure and properties. Springer, Cham. https://doi.org/10.1007/978-3-319-33892-7_2

Hameed BH, Ahmad AA (2009) Batch adsorption of methylene blue from aqueous solution by garlic peel, an agricultural waste biomass. J Hazard Mater 164(2–3):870–875. https://doi.org/10.1016/j.jhazmat.2008.08.084

Hammood ZA, Chyad TF, Al-Saedi R (2021) Adsorption performance of dyes over zeolite for textile wastewater treatment. Ecol Chem Eng S 28(3):329–337. https://doi.org/10.2478/eces-2021-0022

Hamoudi SA, Hamdi B, Brendlé J (2018) Removal of ions Pb^{2+} and Cd^{2+} from aqueous solution by containment geomaterials. Exergetic, energetic and environmental dimensions. Academic Press, Cambridge. https://doi.org/10.1016/B978-0-12-813734-5.00058-5

Heller-Kallai L (2013) Thermally modified clay minerals. In: Developments in clay science, vol 5. Elsevier B.V, p 411–433. https://doi.org/10.1016/B978-0-08-098258-8.00014-6

Herbert Freundlich V (1907) Über die adsorption in Lösungen. Z Phys Chem 57(1):385–470

Hevira L, Zilfa R, Ighalo JO, Aziz H, Zein R (2021) Terminalia catappa shell as low-cost biosorbent for the removal of methylene blue from aqueous solutions. J Ind Eng Chem 97:188–199. https://doi.org/10.1016/j.jiec.2021.01.028

Holliday MC, Parsons DR, Zein SH (2022) Agricultural pea waste as a low-cost pollutant biosorbent for methylene blue removal: adsorption kinetics, isotherm and thermodynamic studies. Biomass Convers Bioref 14(5):6671–6685. https://doi.org/10.1007/s13399-022-02865-8

Hribernik S, Stana Kleinschek K, Rihm R, Ganster J, Fink HP, Sfiligoj Smole M (2016) Tuning of cellulose fibres' structure and surface topography: influence of swelling and various drying procedures. Carbohyd Polym 148:227–235. https://doi.org/10.1016/j.carbpol.2016.04.053

Jang JR (1993) ANFIS: adaptive-network-based fuzzy inference system. IEEE Trans Syst Man Cybern 23(3):665

Johnson RD, Arnold FH (1995) The temkin isotherm describes heterogeneous protein adsorption. Biochimica Et Biophys Acta (BBA)/prot Struct Mol 1247(2):293–297. https://doi.org/10.1016/0167-4838(95)00006-G

Kooh MRR, Thotagamuge R, Chou Chau YF, Mahadi AH, Lim CM (2022) Machine learning approaches to predict adsorption capacity of Azolla pinnata in the removal of methylene blue. J Taiwan Inst Chem Eng 132:104134. https://doi.org/10.1016/j.jtice.2021.11.001

Kuang Y, Zhang X, Zhou S (2020) Adsorption of methylene blue in water onto activated carbon by surfactant modification. Water (switzerland) 12(2):1–19. https://doi.org/10.3390/w12020587

Kumari S, Verma A, Sharma P, Agarwal S, Rajput VD, Minkina T, Rajput P, Singh SP, Garg MC (2023) Introducing machine learning model to response surface methodology for biosorption of methylene blue dye using Triticum aestivum biomass. Sci Rep 13(1):8574. https://doi.org/10.1038/s41598-023-35645-z

Labaran AN, ZangoArmaya'u ZUU, Garba ZN (2019) Rice husk as biosorbent for the adsorption of methylene blue. Sci World J 14(2):66–70

Langmuir I (1917) Contribution from the research laboratory of the general electric com-the constitution and fundamental properties of solids and liquids. II Liquids. JACS 39:1848–1906

Liu Q (2020) Pollution and treatment of dye waste-water. IOP Conf Ser: Earth Environ Sci 514(5):052001. https://doi.org/10.1088/1755-1315/514/5/052001

Makeswari M, Santhi T, Ezhilarasi MR (2016) Adsorption of methylene blue dye by citric acid modified leaves of Ricinus communis from aqueous solutions. J Chem Pharm Res 8(7):452–462

Marszałek J, Żyłła R (2021) Recovery of water from textile dyeing using membrane filtration processes. In Process 9(10):1833. https://doi.org/10.3390/pr9101833

Merino D, Athanassiou A (2023) Alkaline hydrolysis of biomass as an alternative green method for bioplastics preparation: in situ cellulose nanofibrillation. Chem Eng J 454(P4):140171. https://doi.org/10.1016/j.cej.2022.140171

Mittal A, Krishnan L, Gupta VK (2005) Removal and recovery of malachite green from wastewater using an agricultural waste material, de-oiled soya. Sep Purif Technol 43(2):125–133. https://doi.org/10.1016/j.seppur.2004.10.010

Nayak AK, Pal A (2017) Green and efficient biosorptive removal of methylene blue by Abelmoschus esculentus seed: process optimization and multi-variate modeling. J Environ Manage 200:145–159. https://doi.org/10.1016/j.jenvman.2017.05.045

Nayak AK, Pal A (2018) Rapid and high-performance adsorptive removal of hazardous acridine orange from aqueous environment using *Abelmoschus esculentus* seed powder: single- and multi-parameter optimization studies. J Environ Manage 217:573–591. https://doi.org/10.1016/j.jenvman.2018.03.137

Nayak AK, Pal A (2019) Development and validation of an adsorption kinetic model at solid-liquid interface using normalized Gudermannian function. J Mol Liq 276:67–77. https://doi.org/10.1016/j.molliq.2018.11.089

Nayak AK, Pal A (2021) Enhanced adsorption of gentian violet dye from water using lignocellulosic agricultural waste modified with di- And tri-carboxylic acids: Artificial intelligence modeling, practical comprehension, mechanistic and regeneration analyses. J Environ Chem Eng 9(4):105578. https://doi.org/10.1016/j.jece.2021.105578

Nwosu-Obieogu K, Dzarma GW, Ehimogue P, Ugwuodo CB, Chiemenem LI (2022) Textile wastewater heavy metal removal using Luffa cylindrica activated carbon: an ANN and ANFIS predictive model evaluation. Appl Water Sci 12(3):52. https://doi.org/10.1007/s13201-022-01575-w

Oyelude E (2011) Adsorption of methylene blue from aqueous solution using acid modified calotropis procera leaf powder. J Appl Sci Environ 6(4):477–484

Park H, Kim J, Lee YG, Chon K (2021) Enhanced adsorptive removal of dyes using mandarin peel biochars via chemical activation with nh4cl and zncl2. In Water (switzerland). 13(11):1495. https://doi.org/10.3390/w13111495

Panic VV, Madzarevic ZP, Volkov-Husovic T, Velickovic SJ (2013) Poly(methacrylic acid) based hydrogels as sorbents for removal of cationic dye basic yellow 28: Kinetics, equilibrium study and image analysis. Chem Eng J 217:192–204. https://doi.org/10.1016/j.cej.2012.11.081

Patil CS, Kadam AN, Gunjal DB, Naik VM, Lee SW, Kolekar GB, Gore AH (2020) Sugarcane molasses derived carbon sheet@ sea sand composite for direct removal of methylene blue from textile wastewater: Industrial wastewater remediation through sustainable, greener, and scalable methodology. Sep Purif Technol 247:116997. https://doi.org/10.1016/j.seppur.2020.116997

Pavasars I, Hagberg J, Borén H, Allard B (2003) Alkaline degradation of cellulose: mechanisms and kinetics. J Polym Environ 11(2):39–47. https://doi.org/10.1023/A:1024267704794

Philippou K, Evangelou C, Ioannidis I, Pashalidis I (2023) Pine needle–derived biochar adsorbents for removal of Sm(III) and competitive toxic metals from model aqueous matrices. SCENV, vol 4. https://doi.org/10.1016/j.scenv.2023.100053

Qian Y (2016) Sustainable management of water resources. Engineering 2(1):23–25. https://doi.org/10.1016/J.ENG.2016.01.006

Rafatullah M, Sulaiman O, Hashim R, Ahmad A (2010) Adsorption of methylene blue on low-cost adsorbents: a review. J Hazard Mater 177(1–3):70–80. https://doi.org/10.1016/j.jhazmat.2009.12.047

Ramesh K, Gnanamangai BM, Mohanraj R (2021) Investigating techno-economic feasibility of biologically pretreated textile wastewater treatment by electrochemical oxidation process towards zero sludge concept. In J Environ Chem Eng 9(5):106289. https://doi.org/10.1016/j.jece.2021.106289

Revellame ED, Fortela DL, Sharp W, Hernandez R, Zappi ME (2020) Adsorption kinetic modeling using pseudo-first order and pseudo-second order rate laws: a review. In Clean Eng Technol 1:100032. https://doi.org/10.1016/j.clet.2020.100032

Romero-Ocaña I, Delgado NF, Molina SI (2022) Biomass waste from rice and wheat straw for developing composites by stereolithography additive manufacturing. Ind Crop Prod 189:115832. https://doi.org/10.1016/j.indcrop.2022.115832

Sahu N, Nayak AK, Verma L, Bhan C, Singh J, Chaudhary P, Yadav BC (2022) Adsorption of As(III) and As(V) from aqueous solution by magnetic biosorbents derived from chemical carbonization of pea peel waste biomass: isotherm, kinetic, thermodynamic and breakthrough curve modeling studies. J Environ Manag 312:114948. https://doi.org/10.1016/j.jenvman.2022.114948

Said B, Souad M'R, Ahmed EH (2020) A review on classifications, recent synthesis and applications of textile dyes. Inorg Chem Commun 115:107891

Sareen D, Garg R, Grover N (2014) A study on removal of methylene blue dye from waste water by adsorption technique using fly ash briquette. Int J Chem Environ Eng 5(4):610–613

Sawasdee S, Jankerd H, Watcharabundit P (2017) Adsorption of dyestuff in household-scale dyeing onto rice husk. Energy Procedia 138:1159–1164. https://doi.org/10.1016/j.egypro.2017.10.225

Shaikhiev IG (2022) Use of garlic processing by-products to remove pollutants from aqueous media. Biointerf Res Appl Chem 12(4):4518–4528

de Silva RS, Cavalcanti CDAK, de Valle RCSC, Machado RAF, Marangoni C (2021) Understanding the effects of operational conditions on the membrane distillation process applied to the recovery of water from textile effluents. In Process Saf Environ Prot 145:285–292. https://doi.org/10.1016/j.psep.2020.08.022

Siqueira TCA, da Silva IZ, Rubio AJ, Bergamasco R, Gasparotto F, de Paccola EAS, Yamaguchi NU (2020) Sugarcane bagasse as an efficient biosorbent for methylene blue removal: kinetics, isotherms and thermodynamics. Int J Environ Res Public Health 17(2):526. https://doi.org/10.3390/ijerph17020526

Slama HB, Bouket AC, Pourhassan Z, Alenezi FN, Silini A, Cherif-Silini H, Oszako T, Luptakova L, Golińska P, Belbahri L (2021) Diversity of synthetic dyes from textile industries, discharge impacts and treatment methods. Appl Sci (switzerland) 11(14):1–21. https://doi.org/10.3390/app11146255

Solangi NH, Kumar J, Mazari SA, Ahmed S, Fatima N, Mubarak NM (2021) Development of fruit waste derived bio-adsorbents for wastewater treatment: A review. J Hazard Mater vol 416. Elsevier B.V. https://doi.org/10.1016/j.jhazmat.2021.125848

Srinivasan S, Sadasivam SK (2021) Biodegradation of textile azo dyes by textile effluent non-adapted and adapted *Aeromonas hydrophila*. In Environ Res 194:110643. https://doi.org/10.1016/j.envres.2020.110643

Tanhaei B, Esfandyari M, Ayati A, Sillanpää M (2017) Neuro-fuzzy modeling to adsorptive performance of magnetic chitosan nanocomposite. J Nanostruct Chem 7(1):29–36. https://doi.org/10.1007/s40097-016-0211-4

The State of Food and Agriculture 2021 (2021) In the state of food and agriculture 2021. FAO. https://doi.org/10.4060/cb4476en

Urruzola I, Andrés MA, Németh D, Bélafi-Bakó K, Labidia J (2013) Multicomponents adsorption of modified cellulose microfibrils. Desalin Water Treat 51(10–12):2153–2161. https://doi.org/10.1080/19443994.2012.734685

Wahshi FS, Alqahtani MD, Abdulla M, Ramachandran T, Hamed F, Thiemann T (2019) Adsorption of model dyes on recycled silica gel. Proceedings 48(1):10. https://doi.org/10.3390/ecws-4-06439

Wasti A, Ali Awan M (2016) Adsorption of textile dye onto modified immobilized activated alumina. J Assoc Arab Univ Basic Appl Sci 20:26–31. https://doi.org/10.1016/j.jaubas.2014.10.001

Weber G (1995) van't Hoff revisited: enthalpy of association of protein subunits. In J Phys Chem 99(3):1052–1059

Yetgin S, Ulutan S, Balkose D (2015) Methylene blue adsorption from aqueous solutions to flexible poly(vinyl chloride) silica composites. J Vinyl Add Tech 21(1):42–50. https://doi.org/10.1002/vnl.21379

Yusuff AS, Ishola NB, Gbadamosi AO, Epelle EI (2023) Modeling and optimization of hexavalent chromium adsorption by activated eucalyptus biochar using response surface methodology and adaptive neuro-fuzzy inference system. Environ—MDPI 10(3):55. https://doi.org/10.3390/environments10030055

Yuzer B, Selcuk H (2021) Recovery of biologically treated textile wastewater by ozonation and subsequent bipolar membrane electrodialysis process. In Membr 11(11):900. https://doi.org/10.3390/membranes11110900

Zahraa SH, Gzar HA, Shaimaa HH (2021) Evaluation of laboratory submerged membrane bioreactor and reverse osmosis system for treating textile wastewater and reuse. J Phys: Conf Ser 1973(1):012185. https://doi.org/10.1088/1742-6596/1973/1/012185

Zaidi NAHM, Lim LBL, Usman A, Kooh MRR (2018) Efficient adsorption of malachite green dye using artocarpus odoratissimus leaves with artificial neural network modelling. Desalin Water Treat 101:313–324. https://doi.org/10.5004/dwt.2018.21775

Zhang G, Sun Y, Guo Y, Liu J, Wu L, Lin J (2018) The application of pomelo peel as a carrier for adsorption of epigallocatechin-3-gallate. J Sci Food Agric 98(11):4135–4141. https://doi.org/10.1002/jsfa.8931